A New Coplanar-Grid High-Pressure Xenon Gamma-Ray Spectrometer

Scott D. Kiff, *Student Member, IEEE*, Zhong He, *Senior Member, IEEE*, and Gary C. Tepper

***Abstract*—High-pressure xenon (HPXe) gas is a desirable radiation detection medium for many reasons, including its large atomic number, high density, low mean energy to produce an electron-ion pair, and the ability to produce devices with large detection volumes. While past work in HPXe has produced relatively successful detectors with energy resolution at 662 keV as good as approximately 2% FWHM, an expected limitation of these chambers in field operation is resolution degradation due to the vibration of their Frisch grids. Progress on a detector without a Frisch grid is reported in this submission; it is expected that the proposed anode design will provide competitive energy resolution with minimal degradation from mechanical vibration. Simulations accounting for charge carrier statistics, changes in the charge induced on the anode as a function of interaction location, and electronic noise predict a best-case energy resolution of 2.3% FWHM at 662 keV. Experimental data is compared with these simulations.**

***Index Terms*—Coplanar anodes, gas detectors, Geant, ionization chambers, single polarity charge sensing, xenon.**

I. Introduction

HIGH-PRESSURE XENON (HPXe) gas is a desirable radiation detection medium for many reasons, including its large atomic number, high density, low mean energy to produce an electron-ion pair, and the ability to produce devices with large detection volumes. In the past, three main categories of geometries have been developed: parallel plate with a Frisch grid [1], cylindrical without a grid [2], and finally, gridded cylindrical chambers [3]. Cylindrical detectors without a Frisch grid generally have the poorest energy resolution, as expected: the best energy resolution reported is around 4% full width at half maximum (FWHM) at 662 keV [4]. The spectroscopic performance of both geometries of gridded detectors is generally better and has improved steadily, with the best reported results approaching 2% at 662 keV for both the parallel plate [5], [6] and cylindrical [7] geometries. A limitation of these chambers in practice is rather extreme microphonic noise due to Frisch grid vibration. In addition, the construction of Frisch grids can be complicated. The purpose of this paper is to find a successful alternative to the Frisch grid; the technique of coplanar anode grids first reported by Luke [8] is employed.

Manuscript received November 15, 2004; revised September 22, 2005. This work was supported in part by a National Science Foundation Graduate Research Fellowship, and by the U. S. Department of Energy NEER program office.

S. D. Kiff and Z. He are with the University of Michigan, Ann Arbor, MI 48109 USA (e-mail: kiff@umich.edu; hezhong@umich.edu).

G. C. Tepper is with Virginia Commonwealth University, Richmond, VA 23284 USA (e-mail: gtepper@vcu.edu).

Digital Object Identifier 10.1109/TNS.2005.862804

In the coplanar anode technique, the detector's anode is segmented into many strips (or wires in this case), and alternating strips are directly connected to one another to form two independent anodes. Each anode, then, is made of one-half the total number of strips, and while one anode is constructed from strips 1, 3, 5, and so on, the other anode contains strips 2, 4, 6, etc. Usually one of the anodes is biased higher than the other, so that the electrons will always be collected on one set of anode wires, termed the collecting anode. By constructing and operating the detector in such a manner, the induced charge on each of the two anodes is equal through most of the detection volume except very near the anodes, and subtracting the noncollecting anode's preamplifier output signal from the collecting anode's will give a final pulse amplitude that is independent of interaction location inside the detector, assuming electron-ion recombination can be neglected.

Previously-reported HPXe designs employing the coplanar anode technique include: (i) a cylindrical detector with an insulating support rod along the central axis, around which alternating collecting and noncollecting anode wires were wound in a double-helical fashion; (ii) a planar device with anode strips spiraling out of the center of a circular electrode plate toward its outer radius; and (iii) a concept using two anode wires stretched parallel to the detector's central axis, termed the dual-anode cylindrical ionization chamber (DACIC) by its developers, which has a reported energy resolution of 3% FWHM for 662-keV gamma rays while operated in single-anode mode [9], [10]. Even though the DACIC has exhibited some potential for performing spectroscopy without a Frisch grid, there are some aspects of its design and operation that can be improved. For example, because there are only two anode wires, charge induction on the two anodes is not very uniform for large portions of the detection volume. Two other concerns with the DACIC design stem from both of its anodes being at the same potential: if an event occurs near a point equidistant from the two anode wires, charge diffusion could lead to electrons being collected on both anodes, resulting in a reduced pulse amplitude after signal subtraction; and for multi-vertex events, which are quite probable for high gamma-ray energies, interactions occurring on opposite sides of the detector will be collected by opposing anodes, and the true energy deposition will be diminished by the subtraction step.

The focus of this paper is an expansion of the DACIC concept, extending it to an anode structure formed by numerous wires connected into two sets; increasing the number of wires makes the charge induction as a function of interaction position more uniform. The wires run parallel to the central axis of the cylindrical detector, are all positioned at the same radius with re-

TABLE I
SUMMARY OF FIXED DESIGN PARAMETERS

Parameter	*Design Value*
Detection volume length	101.6 mm
Cathode diameter	101.6 mm
Anode displacement from central axis	12.7 mm
Anode wire diameter	1.0 mm
Xenon density	0.3 g/cm^3

spect to the central axis, and have equal spacing separating each wire from its adjacent neighbors. By making connections such that the wires are grouped into two wire sets, they behave as coplanar anodes when operated correctly. In addition, applying a bias difference between the two anodes can alleviate the two concerns with the DACIC design resulting from charge sharing between the anode wires. The proposed design steers all electrons to a designated anode via an applied potential, so these concerns are assuaged.

II. DETECTOR DESIGN AND SIMULATIONS

For the proposed HPXe detector, a previously developed cylindrical detector with helical anodes is refurbished with a new anode design; therefore, the dimensions of the detector are constrained. The variable design parameters are the number of wires (although the number of anodes is always two, the number of wires per anode can be changed); the diameter of the individual wires; and the radius at which the wires are positioned with respect to the detection volume's central axis. For this particular analysis, the diameter of each wire and the radius at which each wire is located are not studied, although in the future these parameters should be considered; only the total number of wires is optimized in this particular design. Table I lists the parameters fixed during design optimization, and Fig. 1 shows a schematic of the proposed design.

A. Optimizing the Number of Anode Wires

To choose the optimal anode configuration and predict the detector's performance, two sets of computational simulations are performed: electrostatic simulations of the weighting potential using the Maxwell 3D code [11], and Monte Carlo simulations of the predicted energy spectra using the Geant4 code [12]. Maxwell 3D simulations of the weighting potential distribution inside the detector allow the induced charge on an anode wire to be calculated using the Shockley-Ramo theorem [13]. The Shockley-Ramo theorem states that the net charge Q induced on a conductor by moving charges q in the detector can be calculated using the weighting potential at position $\mathbf{x}$, $\varphi(\mathbf{x})$

$$\mathrm{Q}(\mathbf{x}) = -\mathrm{q}[\varphi(\mathbf{x}) - \varphi(\mathbf{x_0})]. \tag{1}$$

The weighting potential is found by solving Laplace's equation subject to the boundary conditions $\varphi(\mathbf{x}) = 1$ at all surfaces of the electrode of interest and $\varphi(\mathbf{x}) = 0$ on all other conducting surfaces.

The ideal anode weighting potential distribution is similar to a delta function distribution—zero at all points throughout the volume except at the location of the anode wires of interest, where the weighting potential would rise quickly to unity. A weighting potential of zero at all points outside the anode of interest makes the total induced charge Q independent of interaction location; this can be deduced by examining (1), and setting $\varphi(\mathbf{x}_0) = 0$ and $\varphi(\mathbf{x}) = 1$. In this case, the final induced signal is proportional to the number of *electrons* generated in the radiation interaction, since the positive ions created in the interactions begin and end their paths at locations where the weighting potential is zero, and would thus make no contribution to the anode signal.

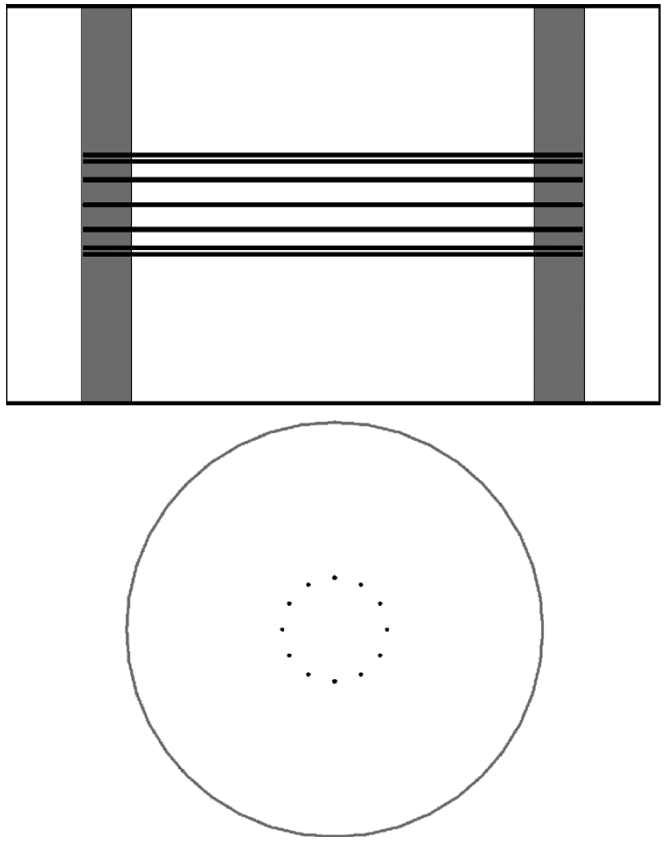

Fig. 1. Schematics of the proposed detector; anode wires are black, Macor structural material is dark gray, and white areas are filled with xenon. Top: a side view. The gas spaces at the ends of the detector are dead volumes. Bottom: a cross-sectional view through the active volume.

In this detector signal subtraction is employed, so the final pulse amplitude $\mathrm{Q_d}$ will be the difference of the induced charge on each preamplifier. Assuming all electron trajectories terminate at the collecting anode, it is straightforward to manipulate (1) to find an expression for $\mathrm{Q_d}$

$$\mathrm{Q_d} = -\mathrm{q}(1 - \varphi_\mathrm{d}). \tag{2}$$

In (2) the weighting potential difference, φ_d, is the difference of the collecting and noncollecting anode weighting potentials at the point of the gamma ray's interaction, $\mathbf{x}_0$. Fig. 2 shows simulated subtracted weighting potential distributions for several anode configurations in the proposed detector. The weighting potential in Fig. 2 is shown along a radial segment that passes through the center of a collecting anode wire; the anode wire is centered at radius 12.7 mm.

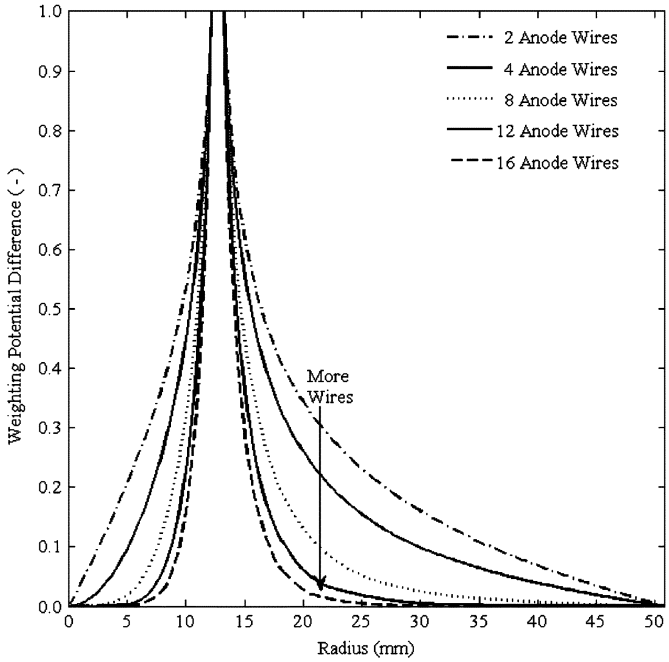

Fig. 2. The effect of varying the number of anode wires is shown in the difference of the collecting and noncollecting anode weighting potentials. This plot shows the weighting potential difference for a radial segment passing through the center of a collecting anode wire. Increasing the number of anode wires from 2 to 16 better approximates an ideal weighting potential distribution.

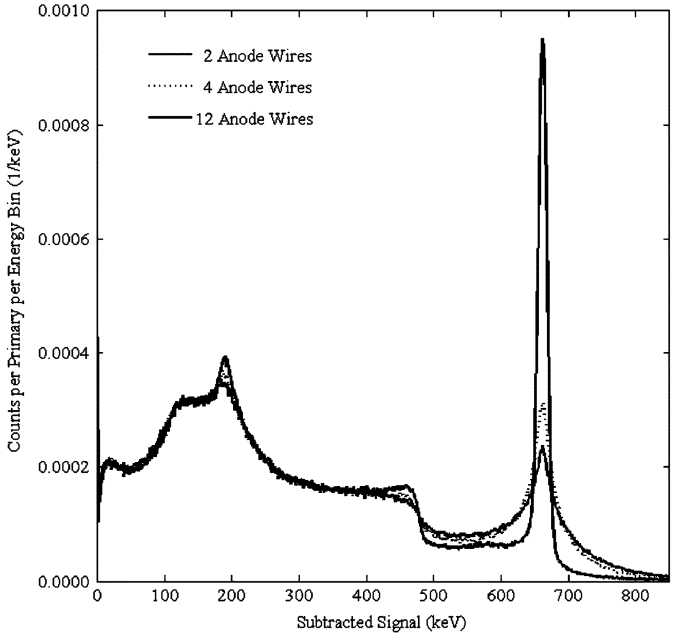

Fig. 3. Geant4 simulated ^{137}Cs spectra. The effect of changing the number of anode wires is shown in the three data series. For 12 wires, the predicted energy resolution is 2.3% FWHM at 662 keV using a 2-μs shaping time.

From Fig. 2, it is obvious that more anode wires translate into a pulse height that is increasingly independent of interaction location. This effect tends to improve energy resolution as more wires are added to the anode structure. However, adding wires increases the preamplifier input capacitance, which increases electronic noise and tends to degrade energy resolution. Thus, it is obvious that the optimal anode structure is some balance of charge induction uniformity and electronic noise, best quantified with Geant4 simulations.

The Geant4 simulations performed to design the optimal anode structure include the effects of Fano statistics, weighting potential difference, and preamplifier electronic noise. The weighting potential distribution used is a Fourier series approximation to the Maxwell 3D simulation results, and accounts for radial and azimuthal variations. The electronic noise is determined as a function of input capacitance from the Amptek A250 specification sheet [14], since the experimental preamplifiers are of this model; the preamplifier input capacitance was calculated to be 22.8 pF using Maxwell 3D. The equivalent noise charge (ENC) given by the Amptek A250 specification sheet is for a shaping time of 2 μs, which is probably not achievable with the current detector, but it will at least allow for consideration of electronic noise effects. To determine the total electronic noise for the system, the ENC for one A250 is multiplied by $\sqrt{2}$ to simplistically account for the use of two preamplifiers in the experiments.

After including all of these effects, simulated spectra are generated for a source of ^{137}Cs gamma rays flooding the end of the pressure vessel. The only physical processes that contribute to the energy spectra in these simulations are Compton scattering and photoelectric absorption of the initial gamma rays; as a result, spectral features unimportant to this study, such as X-ray escape peaks, are absent. Fig. 3 shows the spectral variations as a function of the number of anode wires. The figure only shows a few of the simulated spectra for clarity of presentation.

The result of this analysis is that 12 anode wires (two groups of six wires each) is the optimal configuration for best energy resolution: fewer wires will broaden the photopeak due to larger deviations of the weighting potential from the ideal distribution, while using more than 12 wires leads to wider photopeaks from the associated increase in electronic noise. The spectral feature around 200 keV is the traditional backscatter peak, which comes from the inclusion of the steel pressure vessel and the Macor shell in the Geant4 simulation geometry. The presence of counts at energies greater than the gamma ray's actual energy, also noted in [15], is an artifact of the signal subtraction step. Essentially it is possible for gamma-ray interactions to occur in locations where the net induced charge on the collecting anode is close to the charge generated in the interaction, while the noncollecting anode's induced charge is negative. The subtraction step yields a net signal appearing to be greater than the gamma ray's actual energy, producing a continuum that extends up to double the gamma ray's energy. If Fig. 2 had shown φ_{d} for azimuthal angles near a noncollecting anode wire, negative values of φ_{d} would be shown. Inserting these values into (2) gives artificially high energy measurements.

B. Signal Subtraction Importance

To demonstrate the significance of signal subtraction, let us compare the previous results to simulations of a spectrum formed from the collecting anode's preamplifier signal only. In this case, the weighting potential difference of the two anodes is replaced by just the collecting anode weighting potential, which is much less ideal (see Fig. 4). This effect is somewhat

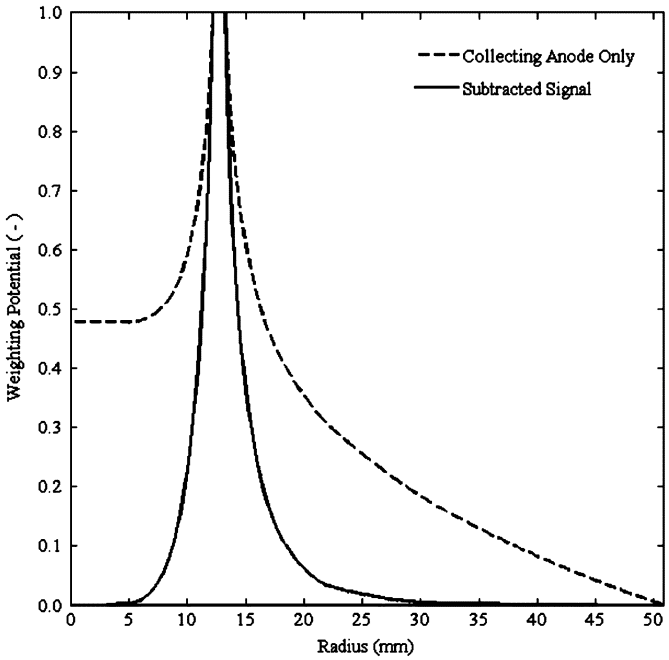

Fig. 4. Comparing the collecting anode's weighting potential distribution to the weighting potential difference used for the subtracted signal. This plot shows the weighting potential for a radial segment passing through the center of a collecting anode wire.

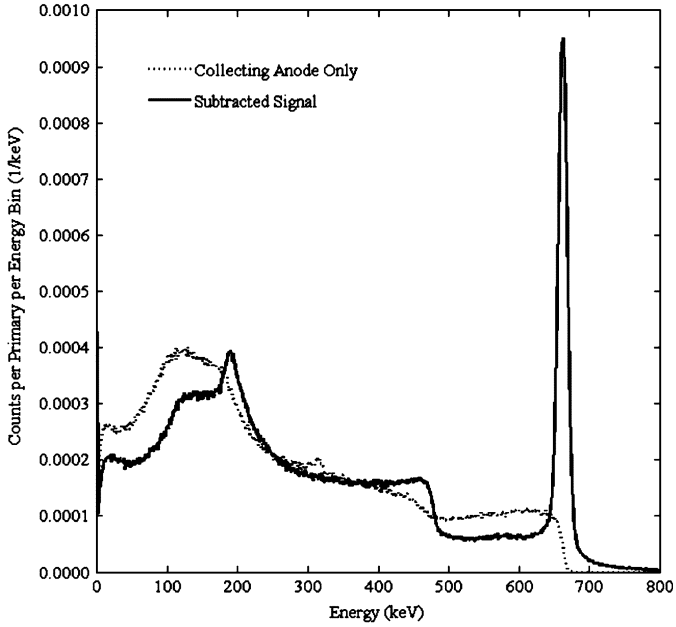

Fig. 5. Simulated ^{137}Cs pulse-height spectra for collecting anode and subtraction circuit signal readout. The collecting anode signal by itself does not even produce a photopeak, whereas signal subtraction produces a photopeak with resolution of 2.3% FWHM at 662 keV when a 2-μs shaping time is considered.

offset by the improved electronic noise, since the subtracted signal noise term is the quadrature sum of the $\sqrt{2}$ noise from both anodes' preamplifiers.

The weighting potential analysis was again simulated using Maxwell 3D. It is interesting to compare Figs. 2 and 4 to note that without signal subtraction, the collecting anode's weighting potential distribution for 12 wires is less ideal than even the two wire case when signal subtraction is employed.

To quantitatively compare the expected pulse height spectra measured from the collecting anode and the subtraction circuit outputs, Geant4 simulations are run with the only differences being: (i) the electronic noise term; and (ii) the weighting potential for induced charge calculations. Fig. 5 displays the results of these two simulations for a ^{137}Cs gamma-ray source irradiating the detector uniformly over one end of the pressure vessel. Note that using only the collecting anode signal is expected to give much worse energy spectra—there is no defined photopeak. Obviously coplanar anodes provide a viable alternative to Frisch grids, but only when signal differencing is employed.

III. Detector Design and Construction

A. Detector Design

As explained in Section II, preexisting HPXe cylindrical chambers incorporating helical anode structures [9] are refurbished with the new anode design in this study. Therefore, many of the design parameters related to the pressure vessel dimensions are constrained. Of the three design parameters that can be varied in this analysis, only the total number of anode wires was optimized. Since the intent of this project is to remove all unnecessary vibrations of the anode structure, sturdy wires are required; a wire diameter of 1 mm has been chosen without any supporting analysis, but it should be optimized in the future for spectroscopic and vibrational considerations. Similarly, the displacement of the anode wires from the detection volume's central axis was fixed throughout the study at a distance known to give an acceptable electric field throughout the detector with the existing power supplies. In the future the effect of wire spacing on detector performance could be examined.

The anode wires are centered at a radius of 12.7 mm relative to the central axis of the chamber. The wires, made of a BeCu alloy, are spaced at 30° intervals along the circumference of the cylindrical shell defined by this radius. Symmetric wire spacing between all 12 wires is important for uniform charge induction.

Fig. 6 shows the anode wires in a test assembly; this picture shows the arrangement of the wires and how connections are made at the end of the detector to cluster the wires into two anodes (collecting and noncollecting groups of six wires each). Fig. 7 shows the anode wires protruding from a Macor structural shell before insertion into the steel pressure vessel. The cathode is a silver film lining the interior of the Macor insulating shell. This design allows the cathode to be biased to a large negative voltage while keeping the pressure vessel grounded.

B. Central Dead Volume

Examination of Figs. 1, 6, and 7 reveals a cylindrical volume inside the anode structure that will have a low operating electric field. Interactions that occur inside this volume are expected to suffer significant ballistic deficit. Fortunately, this low-field region constitutes just a couple of percent of the total active volume, so it is not expected to have much of an impact on the overall energy spectrum.

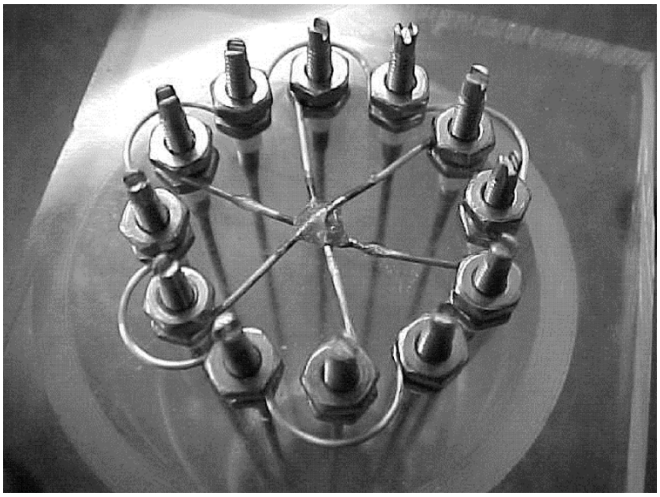

Fig. 6. A view of the anode wires in a test assembly. This picture shows how the twelve anodes wires are connected into two groups, which act as collecting and noncollecting anodes when biased appropriately.

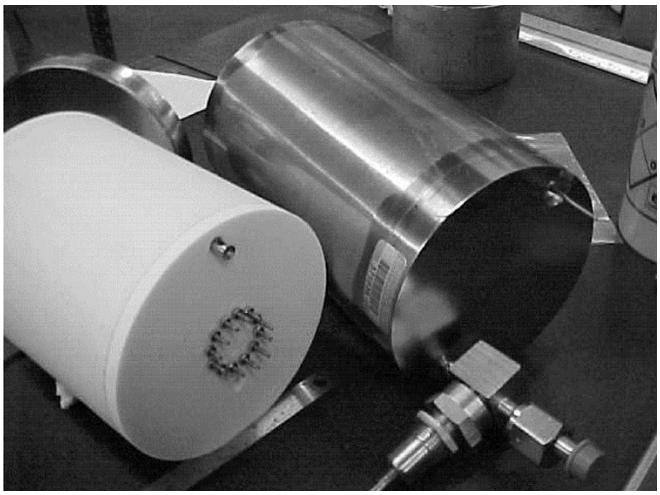

Fig. 7. A view of the detector before final assembly. The white cylinder is the Macor structure that: (i) supports the anodes (protruding from the end); and (ii) supports the cathode, which is a film lining the interior of the Macor shell. The Macor structure is about to be fitted into the pressure vessel from the far end, which will then be welded shut.

C. Xenon Preparation and Detector Filling

The detector baking and filling was performed at a station previously described in [5], but with the xenon purified in a spark purifier. Xenon purification via the spark purification technique is described in [16], and is superior to gettering in terms of final overall gas purity. The detector and the filling station were baked at about 125 °C for several days to accelerate outgassing of the surfaces exposed to xenon, ensuring prolonged purity. The detector was filled to a density of 0.3 g/cm^3, determined by the measured mass of xenon added and the known volume of the detector.

IV. Experiments

The detector was tested with each anode connected to an Amptek A250 preamplifier; preamplifier output differencing was performed with a custom-built subtraction circuit. All experiments use a ^{137}Cs gamma-ray source, and a shaping time of 16 μs is used, as this is the longest setting on the available Canberra 243 amplifier.

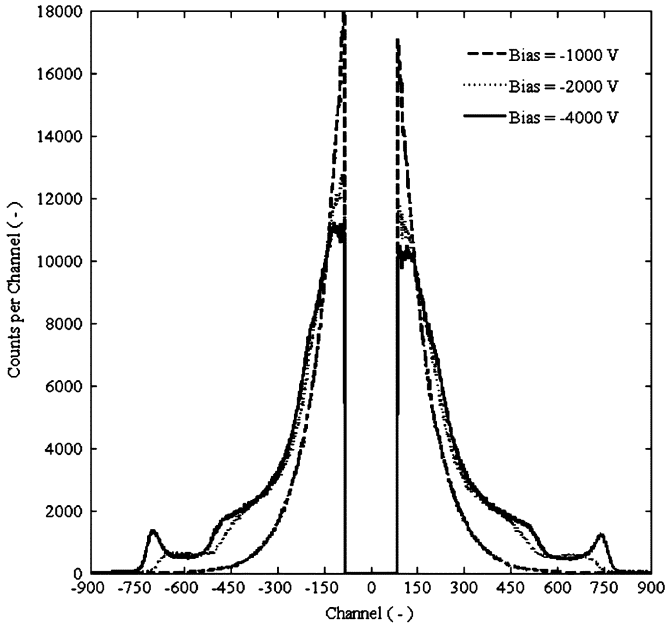

Fig. 8. Experimental pulse height spectra obtained with a ^{137}Cs gamma-ray source. Both anode sets are grounded in these experiments, and the spectra are recorded as the cathode bias is lowered from ground. The negative signals arise from the subtraction circuit, and symmetry about the vertical axis is expected for these spectra.

A. Interelectrode Capacitance Measurements

The capacitance between the two anodes and also between an anode and the cathode were measured experimentally. The procedure used was to input a known test pulse directly onto either the cathode or the noncollecting anode, and then to measure the induced signal on the collecting anode while its bias is set to ground. Thus, the induced charge can be measured, the voltage difference is known, and it is straightforward to calculate the capacitance between two electrodes. The measured capacitance between the cathode and the collecting anode is 1.6 pF, while the capacitance between anodes is 11.7 pF. Thus, the total input capacitance of 13.3 pF for a given preamplifier is significantly less than expected from the Maxwell 3D simulations (22.8 pF).

B. Cathode Biasing Experiments

The purpose of the first set of measurements was to determine the necessary applied cathode bias to ensure complete electron collection and minimize ballistic deficit for all events. This was performed by recording pulse-height spectra at 500-volt intervals and looking for the point at which spectral changes ceased. The collecting and noncollecting anodes are both grounded for this experiment.

Fig. 8 shows a representative subset of the acquired data from this experiment. Note the unusual presentation of the energy spectra—there are counts in negative channel bins. This is because the subtraction circuit allows for negative output pulses, depending on the relative magnitude of the collecting and noncollecting anode signals. Since both anodes are grounded, electrons will not drift preferentially toward one anode or the other.

Furthermore, the wire symmetry makes electrons equally likely to be collected on either anode. Thus, over a large number of interactions, the expected energy spectrum will be symmetric about the vertical axis. The region around the vertical axis has no counts because of the lower-level discriminator (LLD) setting on the multichannel analyzer.

In Fig. 8, the spectra are not quite symmetric about the vertical axis—the potentiometer on the subtraction circuit is not tuned perfectly, so the gain of the noncollecting anode signal is about 5% less than that of the collecting anode. The data for cathode biases beyond -4000 V showed no visible changes in the spectrum, which is probably because the electron drift velocity has saturated near 1 mm/μs [17].

C. Anode Biasing Experiments

Now that an appropriate cathode bias of -4000 V has been established, the next step is to start utilizing the anodes properly and increase the applied bias on the collecting anode (the noncollecting anode is grounded throughout all experiments). The goal is to shape the electric field locally around the anodes such that all electrons drift to the collecting anode wires. One easy way of experimentally determining this point is to collect spectra at regular intervals and plot both the positive and negative portions of the collected data. As the collecting anode bias is increased, electron collection will occur more frequently on the collecting anode than on the noncollecting anode wires, and thus the negative subtracted signal amplitudes will diminish as the positive signal amplitudes increase. Complete charge collection at the collecting anode is realized when the negative portions of the energy spectra cease to change with increasing bias.

Fig. 9 presents a subset of the experimental data. As expected, increasing the collecting anode bias gradually shifts the negative-polarity pulses toward positive energies. For some reason, though, the photopeak FWHM does not seem to improve when the collecting anode bias is raised above 400 V, even though electron collection at the collecting anode is far from complete at that point. Also, the electronic noise contribution, as measured with a test signal, is much larger than the value used in the simulations. This is not surprising, though, as the parallel noise term increases significantly with shaping time, and the experimental shaping time (16 μs) is much longer than the simulated shaping time (2 μs) [18]. The test peak has a width of 32.3 keV, thus placing a lower bound on the energy resolution of 4.9% FWHM. The measured photopeak resolution is 6.8% FWHM at 662 keV (using the ORTEC MAESTRO-32 peak fitting routine) when employing collimators to direct the incident radiation upon the midplane of the detector. Using a manual measurement of resolution gives a much improved result: 5.3% FWHM at 662 keV. This measurement technique first establishes the mean heights of the continua on either side of the photopeak, then the height at the peak centroid. The channels that correspond to half of the net rise on either side of the peak are then determined, and these channels mark the FWHM.

D. Discussion

In Fig. 9, the collected spectra all exhibit a rather extreme change in the Compton continuum height between channels 200 and 400. This effect is present in other published results; for example, refer to [6]. One possible explanation for the effect is related to the slow drift of electrons in xenon gas, expected to be about 1 mm/μs in the high-field region near the anodes and about 0.5 mm/μs near the cathode using published drift velocity data [17]; this agrees with experimentally-observed pulse rise-times of about 50 μs over the 38-mm cathode-anode spacing. In the case of gamma rays that undergo Compton scattering in the xenon and interact two or more times inside the detector, the long drift time of the electrons compared to the pulse shaping time used may cause a significant number of the events to be counted as two small-amplitude pulses instead of being integrated into one large-amplitude pulse: this would shift some events from above the Compton edge to low channels in the Compton continuum.

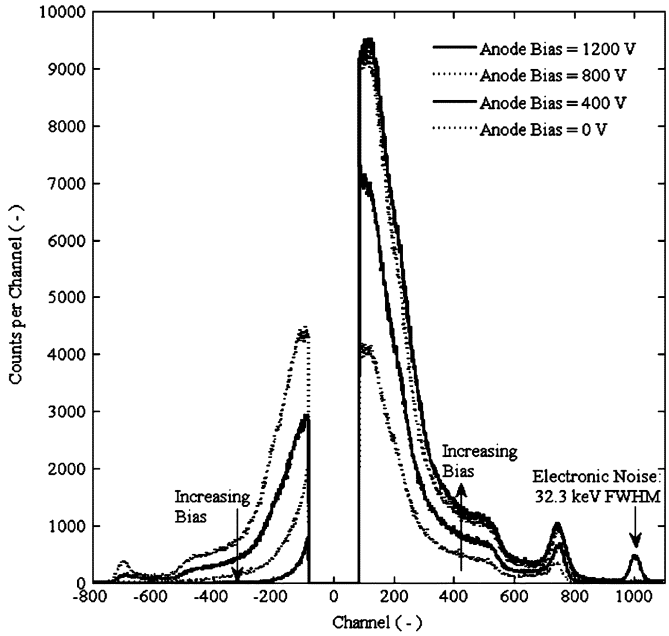

Fig. 9. Experimental pulse height spectra obtained with a ^{137}Cs gamma-ray source. The cathode is held at -4000 V for all measurements, the collecting anode is varied from 0 to 1200 V, and the noncollecting anode is always grounded. The electronic noise is demonstrated by the test signal centered near channel 1000.

The Geant4 simulations presented in Figs. 3 and 5 assume the electron drift time is always significantly shorter than the simulated 2 μs shaping time, so all energy deposited by a given incident photon will be integrated into one signal pulse; this can easily be modified to assume the electron drift time is much longer than the amplifier shaping time so multiple-vertex events will create many signal pulses, not just one. Fig. 10 presents the results of these two simulation extrema, one case assuming very short drift times so that all energy depositions related to a given incoming gamma ray are summed into one count, the other extreme assuming drift times so long that all gamma ray interactions are recorded as separate events in the pulse-height spectrum, even if two or more of these events can be traced to the same incoming gamma ray. Although the long drift time assumption has a noticeable effect on the simulated spectrum by creating the expected changes, the effects are not as severe as shown in the experimental data of Fig. 9.

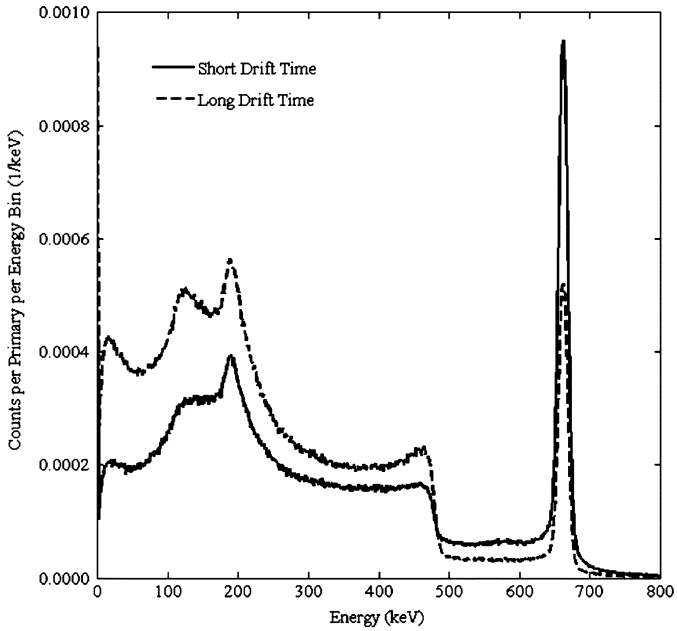

Fig. 10. The effects of long and short electron drift time extrema on simulated ^{137}Cs pulse height spectra.

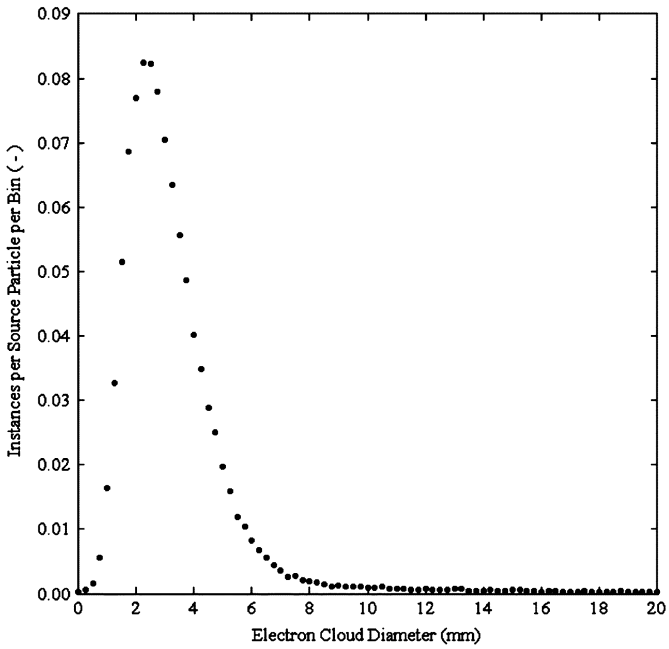

Fig. 11. The initial distance across the cloud of ionized electrons in a fixed direction for a 662-keV photoelectron passing through 0.3 g/cm^3 xenon gas.

Another puzzling feature of the measured spectra is the poor energy resolution. In the Geant4 simulations an assumption was made that the electrons created in gamma-ray interactions were all located at a single point, whereas in reality there will be some initial dispersion of the electron cloud, since the ionizations will be distributed along the paths of the energetic delta rays. The spatial distribution of these electron clouds can be estimated using Geant4 simulations. Fig. 11 presents the simulation results for 662-keV photoelectrons oriented randomly in 0.3 g/cm^3 xenon gas. The data was generated by tracking the position of each ionized electron and then finding the distance between the furthest two electrons along the radial direction. The data was then sorted into 0.250-mm bin widths. While this procedure does not necessarily find the greatest distance between two electrons in the cloud, it is representative of the detector geometry, where the electrons will always drift radially, and the maximum radial separation of ionized electrons will determine the pulse risetime, not azimuthal or axial spread.

From Fig. 11, it is obvious that a very large fraction of photoelectric events will have electron clouds between 1 and 6 mm across in the direction of drift. Let us consider a photoelectric event near the cathode that creates an electron cloud 5 mm across in the direction of drift. The combination of the low drift velocity in this region and the electron spacing could very well cause pulse height deficit in the spectra, which would obviously degrade spectroscopic performance of the detector.

Another consideration for the poor energy resolution is the long shaping time. As discussed previously, the parallel noise contribution to electronic noise increases noticeably as shaping time increases; shortening the shaping time would have the effect of reducing the electronic noise contributions to peak broadening, which could potentially bring the actual performance of the device more in line with the predicted performance if shaping times could be reduced to a few microseconds. One way of achieving this would be to use small hydrogen admixtures to the xenon gas, which have the effect of increasing the electron drift velocity by a factor of up to 5 or more at moderate electric field intensities [19].

V. Conclusion

This paper examined the use of the coplanar anode technique with multiple sturdy wires parallel to the detector's central axis as a suitable alternative to gridded HPXe ionization chambers. For the chosen geometry, electrostatic and Monte Carlo simulations predicted 12 wires grouped into two anode sets of six wires each to be the optimal anode configuration, with a best-case energy resolution of 2.3% FWHM at 662 keV for a shaping time of 2 μs.

The experimental results show that electronic noise is more significant than expected: 32.3 keV as measured with a test pulse, although this can be explained by the increase of parallel noise with longer shaping times. Experiments also found the gain of the noncollecting anode signal relative to the collecting anode signal to be about 5% lower than the optimal condition. Both of these situations can be improved in the future, which will certainly improve the measured energy resolution of 6.8% FWHM at 662 keV (5.3% using a manual measurement technique). Ballistic deficit may contribute significantly to performance degradation, and needs to be considered. Future investigations into the effects of hydrogen admixtures and shaping time studies may be helpful to understand the detector's potential performance.

While the long-term goal of this project is to develop a vibration-resistant ionization chamber, no quantitative vibration studies have been performed at this early stage. However, the ability of this detector to perform measurements next to a running air conditioning unit or while people are working in the

same room is promising, as many gridded detectors are so sensitive to vibration that such environments would severely degrade spectroscopic performance.

ACKNOWLEDGMENT

The authors wish to thank J. Berry of the University of Michigan and R. Unwin of the University of California, San Diego, for assistance with the electrical circuits and mechanical design, respectively. Finally, we express our gratitude to Dr. R. Kessick of Sentor Technologies, Inc. for assistance in gas purification and detector filling.

REFERENCES

[1] V. V. Dmitrenko, A. S. Romanyuk, S. I. Suchkov, and Z. M. Uteshev, "Compressed-xenon ionization chamber for gamma spectrometry," *Instr. Exp. Tech.*, vol. 29, no. 1, pp. 14–17, Jan. 1986.

[2] V. V. Dmitrenko, V. N. Lebedenko, A. S. Romanyuk, and Z. M. Uteshev, "A cylindrical ionization chamber for low-energy (0.1–3 MeV) γ-ray spectrometry," *Instr. Exp. Tech.*, vol. 24, no. 5, pp. 1146–1149, Mar. 1982.

[3] S. E. Ulin, V. V. Dmitrenko, V. M. Gratchev, O. N. Kondakova, S. V. Krivov, S. I. Sutchkov, Z. M. Uteshev, K. F. Vlasik, Y. T. Yurkin, and I. V. Chernysheva, "High pressure xenon cylindrical ionization chamber with a shielding mesh," in *Proc. SPIE 2305—Gamma-Ray Detector Physics and Applications*, 1994, pp. 28–32.

[4] V. V. Dmitrenko, A. E. Bolotnikov, A. M. Galper, V. M. Gratchev, S. E. Ulin, O. M. Kondakova, V. B. Komarov, S. V. Krivov, S. I. Suchkov, Z. M. Uteshev, Y. T. Yurkin, and K. F. Vlasik, "High pressure xenon filled cylindrical gamma-ray detector," in *Proc. SPIE 1734—Gamma-Ray Detectors*, 1992, pp. 295–301.

[5] G. Tepper and J. Losee, "High resolution room temperature ionization chamber xenon gamma radiation detector," *Nucl. Instrum. Meth. A*, vol. 356, no. 2–3, pp. 339–346, Mar. 1995.

[6] G. J. Mahler, B. Yu, G. C. Smith, W. R. Kane, and J. R. Lemley, "A portable gamma-ray spectrometer using compressed xenon," *IEEE Trans. Nucl. Sci.*, vol. 45, no. 3, pp. 1029–1033, June 1998.

[7] A. Bolotnikov and B. Ramsey, "Improving the energy resolution of high-pressure Xe cylindrical ionization chambers," *IEEE Trans. Nucl. Sci.*, vol. 44, no. 3, pp. 1006–1010, June 1997.

[8] P. N. Luke, "Single-polarity charge sensing in ionization detectors using coplanar electrodes," *Appl. Phys. Lett.*, vol. 65, no. 22, pp. 2884–2886, Nov. 1994.

[9] C. J. Sullivan, Z. He, G. F. Knoll, G. Tepper, and D. K. Wehe, "A high pressure xenon gamma-ray spectrometer using a coplanar anode configuration," *Nucl. Instrum. Methods A*, vol. 505, no. 1–2, pp. 238–241, Jun. 2003.

[10] A. Bolotnikov, A. Bolozdynya, R. DeVito, and J. Richards, "Dual-anode high-pressure xenon cylindrical ionization chamber," *IEEE Trans. Nucl. Sci.*, vol. 51, no. 3, pp. 1262–1269, Jun. 2004.

[11] *Maxwell 3D*, 2003. ver. 9.

[12] *Geant4*, 2003. ver. 4.5.

[13] Z. He, "Review of the Shockley-Ramo theorem and its application in semiconductor gamma-ray detectors," *Nucl. Instrum. Methods A*, vol. 463, no. 1–2, pp. 250–267, May 2001.

[14] A250 Product Specification Sheet (2003, Sep.). [Online]. Available: http://www.amptek.com/pdf/a250.pdf

[15] Z. He, G. F. Knoll, D. K. Wehe, and J. Miyamoto, "Position-sensitive single carrier CdZnTe detectors," *Nucl. Instrum. Meth. A*, vol. 388, no. 1–2, pp. 180–185, Mar. 1997.

[16] A. Bolotnikov and B. Ramsey, "Purification techniques and purity and density measurements of high-pressure Xe," *Nucl. Instrum. Methods A*, vol. 383, no. 2–3, pp. 619–623, Dec. 1996.

[17] J. L. Pack, R. E. Voshall, and A. V. Phelps, "Drift velocities of slow electrons in krypton, xenon, deuterium, carbon monoxide, carbon dioxide, water vapor, nitrous oxide, and ammonia," *Phys. Rev.*, vol. 127, no. 6, pp. 2084–2089, Sept. 1962.

[18] G. F. Knoll, *Radiation Detection and Measurement*, 3rd ed. New York: Wiley, 2000, pp. 631–632.

[19] S. E. Ulin, V. V. Dmitrenko, V. M. Grachev, Z. M. Uteshev, K. F. Vlasik, I. V. Chernysheva, A. G. Dukhvalov, F. G. Kotler, and K. N. Pushkin, "Gamma-detectors based on high pressure xenon: Their development and application," in *Proc. SPIE 5540—Hard X-Ray and Gamma-Ray Detector Physics VI*, 2004, pp. 248–256.